Journal of Alloys and Compounds 763 (2018) 899–908

Contents lists available at ScienceDirect

Journal of Alloys and Compounds

journal homepage: http://www.elsevier.com/locate/jalcom

Study of ultrathin Pt/Co/Pt trilayers modified by nanosecond XUV pulses from laser-driven plasma source

I. Jacyna [a], D. Klinger [a], J.B. Pełka [a], R. Minikayev [a], P. Dłużewski [a], E. Dynowska [a], M. Jakubowski [a], M.T. Klepka [a], D. Zymierska [a], A. Bartnik [b], Z. Kurant [c], A. Wolska [a], A. Wawro [a], I. Sveklo [c], J.R. Plaisier [d], D. Eichert [d], F. Brigidi [d], I. Makhotkin [e], A. Maziewski [c], R. Sobierajski [a, *]

[a] Institute of Physics, Polish Academy of Sciences, 02- 668 Al. Lotników 32/46, Warsaw, Poland
[b] Institute of Optoelectronics, Military University of Technology, ul. gen. S. Kaliskiego 2, 00-908, Warsaw, Poland
[c] Laboratory of Magnetism, Faculty of Physics, University of Bialystok, K. Ciolkowskiego 1L, 15-245, Bialystok, Poland
[d] Elettra-Sincrotrone Trieste, S.S. 14 Km 163.5 in Area Science Park, 34149, Basovizza, Trieste, Italy
[e] MESA+ Institute for Nanotechnology, University of Twente, Netherlands

ARTICLE INFO

Article history:
Received 15 December 2017
Received in revised form
16 May 2018
Accepted 25 May 2018
Available online 26 May 2018

Keywords:
Ultrathin Pt/Co/Pt films
Magnetic reorientation
XUV irradiation
Atomic diffusion
Alloys formation

ABSTRACT

We have studied the structural mechanisms responsible for the magnetic reorientation between in-plane and out-of-plane magnetization in the (25 nm Pt)/(3 and 10 nm Co)/(3 nm Pt) trilayer systems irradiated with nanosecond XUV pulses generated with laser-driven gas-puff target plasma source of a narrow continuous spectrum peaked at wavelength of 11 nm. The thickness of individual layers, their density, chemical composition and irradiation-induced lateral strain were deduced from symmetric and asymmetric X-ray diffraction (XRD) patterns, grazing-incidence X-ray reflectometry (GIXR), grazing incidence X-ray fluorescence (GIXRF), extended X-ray absorption fine structure (EXAFS) and transmission electron microscopy (TEM) measurements. In the *as grown* samples we found, that the Pt buffer layers are relaxed and that the layer interfaces are sharp. As a result of a quasi-uniform irradiation of the samples, the XRD, EXAFS, GIXR and GIXRF data reveal the formation of two distinct layers composed of $Pt_{1-x}Co_x$ alloys with different Co concentrations, dependent on the thickness of the *as grown* magnetic Co film but with similar ~1% lateral tensile residual strain. For smaller exposure dose (lower number of accumulated pulses) only partial interdiffusion at the interfaces takes place with the formation of a tri-layer composed of Co-Pt alloy sandwiched between thinned Pt layers, as revealed by TEM. The structural modifications are accompanied by magnetization changes, evidenced by means of magneto-optical microscopy. The difference in magnetic properties of the irradiated samples can be related to their modification in $Pt_{1-x}Co_x$ alloy composition, as the other parameters (lateral strain and alloy thickness) remain almost unchanged. The out-of-plane magnetization observed for the sample with initially 3 nm Co layer can be due to a significant reduction of demagnetization factor resulting from a lower Co concentration.

1. Introduction

It is well known that some ultrathin film systems containing magnetic 3d metal (e.g. Co, Fe) interleaved with a non-magnetic material exhibit tunable magnetization reorientation between in-plane and out-of-plane directions. The Pt/Co/Pt system is particularly interesting due to strong anisotropy and magnetic polarization of nonmagnetic atoms at Co-Pt interfaces. Different remarkable phenomena, such as enhanced magneto-optic effect [1], induced magnetic moment [2,3], extraordinary Hall effect [4], etc. have been observed. The presence of perpendicular magnetization triggered further the research interest in Pt/Co/Pt magnetic anisotropy [5,6], spin reorientation transition [7] magnetic domains [8,9], and magneto-optical response in the ultraviolet range [10]. A spin reorientation transition (SRT) between in-plane and out-of-plane magnetization was evidenced in Pt/Co/Pt structures when irradiated with ion beams and light pulses of different photon energy. In particular, the ultrafast annealing with optical lasers leads to

* Corresponding author.
E-mail address: ryszard.sobierajski@ifpan.edu.pl (R. Sobierajski).

https://doi.org/10.1016/j.jallcom.2018.05.314
0925-8388/

structural and magnetic changes at the magnetic Co film and its interfaces, without overheating of the substrate. This is important for thin film technological applications, especially for spintronic and magneto-optical memory technologies. It is considered that magnetic properties of a system containing single, ultrathin Co film result mainly from the structural features of the film system and its interfaces. SRT obtained by irradiations is mostly controlled by the contribution of the interfaces modifications with strain formation and symmetry breaking (see, e.g., [11–13]). A few years ago, magnetization switching in Co-Pt structures [14,15] and multiple SRT [16,17] induced by the light irradiation were observed. This finding has revived the importance of the structural background in magnetic phenomena and its sensitivity to external factors, as even small variations in ion or laser irradiation parameters, which would create optimal conditions for the material properties engineering. Magnetic anisotropy in Pt/Co/Pt can be controlled with different parameters such as Co film thickness or samples growth temperature. It is important to optimize methods for magnetic properties patterning. Ion beam or light irradiations are used for these purposes. In general, sample irradiation may lead to such phenomena as blurring of originally sharp interfaces and, as a result of atomic interdiffusion, formation of a PtCo chemically disordered and ordered alloys, together with the appearance of defects and strains. Such structural modifications can change the basic magnetic properties of multilayer structures – specifically magnetic anisotropy. In particular, interface blurring may reduce the surface anisotropy, while atomic interdiffusion may lead to formation of alloys with specific magnetocrystalline anisotropy. In case of lattice deformation – magneto-elastic anisotropy contribution may become significant, as well.

It has been shown by Chappert et al. [18] that 30 keV He + ions irradiation can reduce magnetic anisotropy for thin Co films, of thickness d_{Co}, and magnetization rotates to in-plane state without a visible change of surface morphology. Structural studies [19,20] suggest that irradiation destroys Co/Pt interface, which in turn induces substitutional mixing maintaining the initial crystallographic structure but reducing magnetic anisotropy. Successively was demonstrated that for thick Co films ($d_{Co} > d_{SRT}$, where d_{SRT} is the thickness of Co layer when SRT occurs), an increase of magnetic anisotropy occurs upon 30 keV Ga + ion irradiation [21,12]. Structural studies by Sakamaki et al. [22] claims that the increase of magnetic anisotropy is correlated with the increase of surface tensile strain under ion irradiation.

Laser annealing at nanoseconds pulse duration range was performed on multilayer (0.3 nm Co)/(0.8 nm Pt) film [23]. At lower laser intensities, where no ordered alloy formation is observed, the magnetization saturation has increased by 10% while the effective magnetic anisotropy decreased by about 50%. At higher laser intensities, the appearance of new broad XRD reflection indicates the formation of a Co–Pt chemically disordered alloy. For thicker Co films ($d_{Co} > d_{SRT}$), femtosecond pulse laser irradiation can induce the increase of magnetic anisotropy [16]. Similar effect induced by extreme ultraviolet (XUV) light pulses also exists in Pt/Co/Pt.

In our previous report, the intermixing effect giving rise to the creation of Co_xPt_{1-x} chemically disordered alloy induced in ultrathin (5 nm Pt)/(3 nm Co)/(5 nm Pt) trilayer system by raster irradiation with intense XUV light pulses was demonstrated by XRD and supported with TEM measurements [24]. In this paper the approach to determine the strain properties, the relaxed lattice parameters of the unit cell and the Pt-Co alloy composition in the system, was also described. In another work [25] the radial dependence of remanence, coercivity and saturation fields across the irradiated spots were studied with aid of magneto-optical techniques for the samples with various Co (0.5–10 nm) and Pt buffer (5 and 40 nm) layer thicknesses (AFM and MFM). The sample surface and magnetic ordering were investigated using atomic force and magnetic force microscopies. However, no measurements of structural parameters like the atomic diffusion or strain were included in the study. Instead, based on magnetic and morphological changes, the residual stress after thermoplastic deformation in the spot area was discussed as a reason for the observed transformation.

In the present work, we report on structural properties investigation of ultrathin Pt/Co/Pt system with Pt buffer film of a thickness of 25 nm modified by irradiation with XUV nanosecond pulses. The main objective of the study is to further clarify questions related to the structural background of the observed magnetic phenomena in the systems. Following the observation by E. Dynowska et al. [24] of atomic interdiffusion at interfaces accompanied by the formation of $Pt_{1-x}Co_x$ alloys, we studied their influence on changes in sample composition (depth concentration profile), strain and magnetization. We have further investigated down to which depth some modifications can potentially occur, as well as the possible differences in case of single and multiple pulse irradiations. The later problem was partly addressed by Sveklo et al. [25], who, however restricted their study to morphological and magnetic measurements. In our present study, we have chosen samples with different layer structures (thicker Pt buffer layer, various Co layer thickness), more suitable for our purposes. Thicker layers allow the formation of composition gradients in the final alloys varying significantly from what was previously observed. Moreover, we complement our investigations by combining structural methods such as XRD with EXAFS, GIXR and GIXRF techniques that allow to investigate the structure of layers and interfaces with high precision, regardless of their crystal arrangement.

2. Materials and methods

The Pt/Co/Pt samples are described in Table 1. The thickness of the Co layer in the structure S03 was 3 nm, while in S04 it was 10 nm. The samples were deposited on sapphire (0001) substrates of $10 \times 10 \times 0.5\ mm^3$ size, using molecular beam epitaxy (MBE) at the Institute of Physics PAS in Warsaw. During the same deposition process, several samples of the same structure were grown. The MBE process was carried out at a pressure below 10^{-9} torr, and was monitored *in situ* by RHEED. The substrates were annealed before deposition at 850 °C for 0.5 h. The deposition of the first platinum layer, the "buffer", on the substrate was done at 750 °C. Following Co and Pt cap layers were deposited at room temperature. The *as grown* sample structures were confirmed by XRD, GIXR and GIXRF before irradiation.

The samples were irradiated with the XUV pulses generated by a laser-driven gas-puff target plasma source at the Military University of Technology in Warsaw. The Kr/Xe/He gas target was excited by a 0.8 J Nd:YAG 1–10 Hz laser. The XUV radiation was focused

Table 1
Sample description.

LABEL	Composition [nm]	SAMPLE Irradiation conditions and peak fluence
S03	//Pt 25/Co 3/Pt 3/	A – *as grown* C – 73 mJ/cm^2 (QU)
S04	//Pt 25/Co 10/Pt 3/	A – *as grown* B – 1 × 73 mJ/cm^2 (SA) B – 10 × 73 mJ/cm^2 (SA) C – 73 mJ/cm^2 (QU)

QU – irradiated quasi-uniformly; SA – Spot array irradiation; A..C – samples grown together in one MBE run.

using a gold-plated grazing incidence ellipsoidal collector allowing for efficient focusing of radiation in the $\lambda = 9–70$ nm wavelength range. This source produces intense pulses of radiation in an XUV broadband spectral range, characterized by intense narrow emission maximum at approximately 11 nm, 4 ns pulse duration (FWHM), and 100 μJ maximum pulse energy. After focusing, a Gaussian spot size of 0.5–1 mm was achieved in the focal plane. The maximal achievable peak fluence of the irradiation of the samples with a single pulse was 73 mJ/cm^2. The pulse-to-pulse intensity repeatability was better than 10% [26,27]. Compared to irradiation with femtosecond IR lasers, the XUV photons from the gas-puff target plasma source are absorbed over larger depths, reaching up to the sapphire substrate and heating it. For radiation wavelength of $\lambda = 11$ nm, used for irradiation in the present work and [24,25], the absorption depths for the materials of the samples are: $\zeta_{Pt} = 35.5$ nm, $\zeta_{Co} = 19.7$ nm and $\zeta_{Saph} = 29.7$ nm, for Pt, Co and sapphire substrate, respectively [28]. Moreover, the nanosecond pulse duration gives time for the partial heat dissipation, that further increases depth penetration of the energy and lowers the temperature gradients. Thus the applied pulse duration and spectral range provide excitation condition which are better defined over the whole thickness of the metallic layers, as compared to irradiation with femtosecond IR pulses leading to large temperature gradients and ultrafast energy transport phenomena.

Two irradiation modes were applied to the samples, as illustrated in Fig. 1. The first (Spot Array, SA) produced on the surface a regular matrix of spots separated so that adjacent exposure regions ("spots") do not influence one another. The irradiation parameters in the individual points differed by single shot peak fluence as well as by the number of accumulated shots - 1 to 100 (see Fig. 1a). This type of sample, with a radial distribution of absorbed dose around the spot center, was suitable for investigation with various microscopic techniques from magnetic and optical microscopes to transmission electron microscopy (TEM). The second mode of irradiation, called here the Quasi-Uniform (QU), consisted in exposing large sample surfaces with regular, quasi-continuous raster pattern of partially overlapping spots, with neighboring centers shifted by an amount less than their radii in order to achieve a quasi-uniform irradiated area (see Fig. 1b). In both irradiation modes, the irradiation fluencies were selected to induce the out-of-plane magnetization state. The repetition rate was small enough (1 Hz) to avoid heat accumulation from consequential pulses.

To characterize the sample structures, the XRD, EXAFS, GIXR and GIXRF methods were applied. XRD measurements were performed using PANalytical Empyrean X-ray diffractometer equipped with Cu $K\alpha_1$ radiation ($\lambda = 0.1540598$ nm), a Johansson monochromator Ge(111) in the incident beam and a linear semiconductor strip detector. The GIXR measurements were carried out with a laboratory diffractometer at the MESA + Institute for Nanotechnology, University of Twente in Netherlands, with an excitation energy provided by Cu $K\alpha_1$ X-ray source. The experimental data were analyzed by using X'Pert Reflectivity (ver.1.3) commercial program.

XRD measurements were also performed on the samples at the MCX beamline at ELETTRA – Sincrotrone Trieste using synchrotron radiation at the wavelength of $\lambda = 0.154098$ nm, in order to compare easily the synchrotron and laboratory measurements. Due to adjustment properties of the diffractometer at MCX, all the diffraction measurements have been performed in the sample spinning mode. A comparison of XRD patterns obtained with synchrotron radiation (SR) and with laboratory X-ray diffractometers did not show any significant differences.

GIXRF (together with GIXR) measurements were performed at the X-ray Fluorescence beamline at ELETTRA – Sincrotrone Trieste using a monochromatized synchrotron radiation at exciting photon energies of 8 and 12 keV, i.e. above Co K-edge and Pt L_3-edge, respectively. The beam size was in the order of 250 by 100 μm (hor. by ver.), and in grazing incidence geometry the beam footprint was longer than the sample (>10 mm). The 7 axis manipulator allows for theta/2theta scans with high angular precision (better than 0.005 deg), which enables simultaneous XRR and GIXRF studies of very thin samples (several nm layer thickness). In grazing incidence conditions, the incident beam is successively reflected at the surface of the layers and at the substrate, and an X-ray standing wave is created, giving access to the element compositional profile of the material.

The Extended X-ray Absorption Fine Structure (EXAFS) was measured at the BM08 beamline at the ESRF. The signal was gathered at the Co K-edge in a fluorescence mode at 77 K in a normal (15° incidence angle, probing in-plane bonds parallel to the sample's surface) and grazing (75° incidence angle, probing out-of-

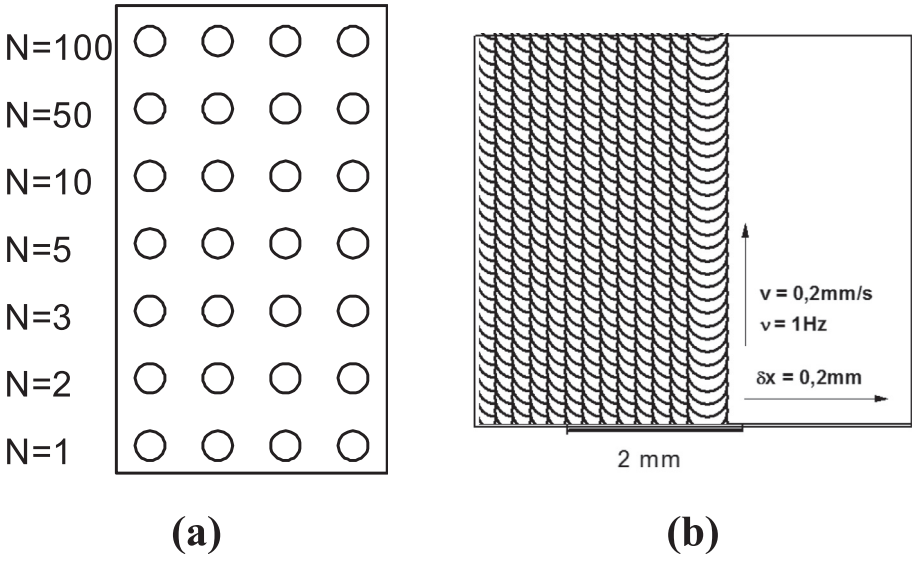

Fig. 1. Sketch explaining two irradiation schemes of sample surface: (a) irradiation in separated discrete places (Spot Array, SA), (b) raster irradiation by steps smaller than the single spot diameter (quasi-uniform, QU).

plane bonds perpendicular to the sample's surface) incidence configurations (full scheme can be found in Ref. [29]).

The optical examination and mapping of irradiated sample surfaces was performed using interference-polarizing microscopy with Nomarski contrast. The same treatment was applied to the *as grown* samples, before irradiation. The structure of the samples was examined by TEM methods using FEI Titan CUBED 80–300 microscope operating at 300 kV acceleration voltage. The cross-sectional specimens were prepared with the use of Focused Ion Beam (FIB) method. To protect the sample surface from damage related to the FIB cutting, the top surface was first covered with a polycrystalline platinum film. In addition, the depth profiles of atomic compositions were obtained in TEM by recording the EDX signal in the investigated sample cross-sections using *in vacuum* detector and excitation with a focused electron beam.

The magnetic properties of Pt/Co/Pt structures before and after irradiation were probed with a polar magneto-optic Kerr effect (P-MOKE) microscope sensitive to out-of-plane magnetization component [13,22]. This system enables imaging of magnetization as a function of the external magnetic field $H_{\perp}$ applied in the direction perpendicular to the sample plane. It was possible to measure locally hysteresis curves with an optical lateral resolution by taking a sequence of images while sweeping the external magnetic field. These curves in each pixel were recorded simultaneously. In spite of a very high sensitivity and good lateral resolution of the MOKE measurements, this method gives a depth averaged result.

3. Results and discussion

In Fig. 2, the X-ray diffraction patterns obtained at the MCX station of ELETTRA Sincrotrone in Trieste for two Pt/Co/Pt structures (designated as S03 and S04) are compared. In the left-column, spectra are presented for 2θ angles within the range of 25–50 deg., consisting of Pt 111 and Sapphire 0006 reflections, while in the right column – within the range of 75–110 deg, with the second order reflections from Pt and Sapphire 00012 substrate. The *as grown* structures are indicated with "A" while structures quasi-uniformly irradiated by XUV pulses are indicated with "C". The *as grown* sample S03 and S04 structures differ only in the central Co film thickness. To get information about strain in Pt films we had to measure additionally an asymmetric Pt reflection. Due to geometrical constrains of the goniometer at MCX, we had to use for this purpose a high-resolution laboratory diffractometer. By calculations based on measured symmetric Pt 222 and (not shown here) asymmetric Pt 113 reflections, we found that platinum in the two layers of sample S03A is relaxed, and the lattice parameter was calculated to be, $a_{rel} = 3.926$ (4) Å, slightly higher than the lattice parameter in a bulk Pt ($a_{Pt} = 3.923$ Å). Similar value of the relaxed lattice parameter of platinum, $a_{rel} = 3.930$ (4) Å, was calculated for sample S04A. The methodology of determination a relaxed lattice parameters as well as isotropic biaxial stress states was detailed described elsewhere [24,30]. The thickness of a buffer layers in the samples S03A (~25.5 nm) and S04A (*t*~26 nm) were estimated on the base of Laue oscillations visible in the vicinity of 111 Pt reflection (Fig. 2) what testifies to the high quality of their interfaces.

In sample S03A the estimated interplanar spacing for the Co peak, visible at 2θ angle ~97,3°, was found to be $d = 1.026$ (2) Å. In sample S04A, as the thickness of the Co layer is 10 nm, we see relatively strong two peaks from Co, (at the 2θ angles 44.3° and 97.9°) – the calculated interplanar spacing are $d_1 = 2.043$ (2) Å and $d_2 = 1.021$ (2) Å, respectively (Fig. 2). On the base of this measurement the crystal structure of the Co cannot be unambiguously identified because the angle-positions of both the 222 fcc and 0004 hcp reflections from Co are very close.

In the irradiated sample S03C we can see, in the angular range near to the nominal positions of the Pt 111 and Pt 222 peaks, two diffraction peaks, marked W1 and W2, very close to one another. The observed shift of the peaks towards higher angles with respect to the expected position as of pure platinum peak indicates that there are two pronounced layers of $Pt_{1-x}Co_x$ alloy of different composition. Due to the fact that, in the XRD of S03C, the peak W1 is indistinct and lies very close to the peak W2 we failed to determine precisely the positions of 222 and 113 peak in the layer W1. In case of layer W2 there were no such problems and the calculated relaxed lattice parameter a_{rel} is equal 3.895 (4) Å. This value corresponds to an alloy $Pt_{0.88}Co_{0.12}$ [24]. Using suitable fitting procedures, it can be estimated however, that the peak W1 corresponds to a thin layer platinum with the lattice parameter $a = 3.930$ (4) Å. A lack of Laue oscillations indicates that there are insufficiently smooth interfaces after irradiation procedure. The composition corresponding to W1 and W2 peaks can be evaluated assuming the *as grown* sample structure (here 28 nm Pt and 3 nm Co) and interplanar spacing in these metals in the direction [111] (d_{111}(Pt) = 2.269 Å and d_{111}(Co fcc) = 2.052 Å). Then we can calculate the number of (111) planes (we get ~123 planes of Pt and ~15 planes of Co). The stoichiometric ratio for the $Pt_{0.88}Co_{0.12}$ alloy is equal 12/88 = 0.136 what corresponds to a structure consisting of the 15 planes of Co and 110 planes of Pt since 15/110 = 0.136 (assuming that all Co atoms are involved in the alloy). It means that 13 planes (3 nm) of Pt remained what confirms correct identification of W2 layer and explains relatively large width of W1 reflection and its low intensity.

In case of irradiated sample S04C, two diffraction peaks, W1 and W2, are visible at a longer distance to one another. Basing on the measured symmetric 222 and asymmetric 113 reflections it was found that the values of the relaxed lattice parameters for W1 and W2 are, $a_{rel} = 3.923$ (4) Å (pure Pt) and $a_{rel} = 3.763$ (4) Å (alloy $Pt_{0.46}Co_{0.54}$), respectively. A lack of Laue oscillations indicates that there are no smooth interfaces in this sample. According to the above described discussion, in this sample we have ~123 (111) planes of Pt and ~49 planes of Co. This means that all Co and 42 planes of Pt form the $Pt_{0.46}Co_{0.54}$ alloy. The remaining 81 planes of Pt form a pure Pt film of thickness ~18 nm. It is a relatively thick layer, hence the W1 peak is relatively narrow with high intensity. The results of XRD investigation for the S03 and S04 structures are collected in Table 2. In the last two columns of Table 2 the stress states values (ε_{xx} and ε_{zz}) calculated based on XRD measurements are shown. These calculations were made on the basis of hexagonal unit cell chosen for structural characterization of the studied layers [24] – the values of the lattice spacing of the planes parallel (*a*) and perpendicular (*c*) to the growth direction for strained and relaxed hexagonal unit cells were used according to the formulas:

$$\varepsilon_{zz} = \frac{c_{strained} - c_{relaxed}}{c_{relaxed}} \text{ and } \varepsilon_{xx} = \frac{a_{strained} - a_{relaxed}}{a_{relaxed}},$$

where *a* and *c* – lattice parameters of the hexagonal unit cells.

The *as grown* structure of the sample S04A (N0), as well as the same structures irradiated in spots by 1 pulse and 10 pulses of XUV radiation of peak fluence 73 mJ/cm^2 (N1 and N10, respectively), were investigated by TEM and are shown in Fig. 3. Slices were cut out of samples with FIB perpendicularly to their surfaces, in homogenous centers of the irradiated spots. In the right part of Fig. 3. TEM pictures are shown and in the right part, the corresponding in-depth distribution profiles of elements obtained by *in situ* EDX detector are shown in the left. In the *as grown* sample (bottom row) Pt buffer layer grown at 750 °C shows high uniformity and sharp interface with Co layer. However, the Pt-Co lattice mismatch leads to Co thickness lateral undulations which result in the waviness of

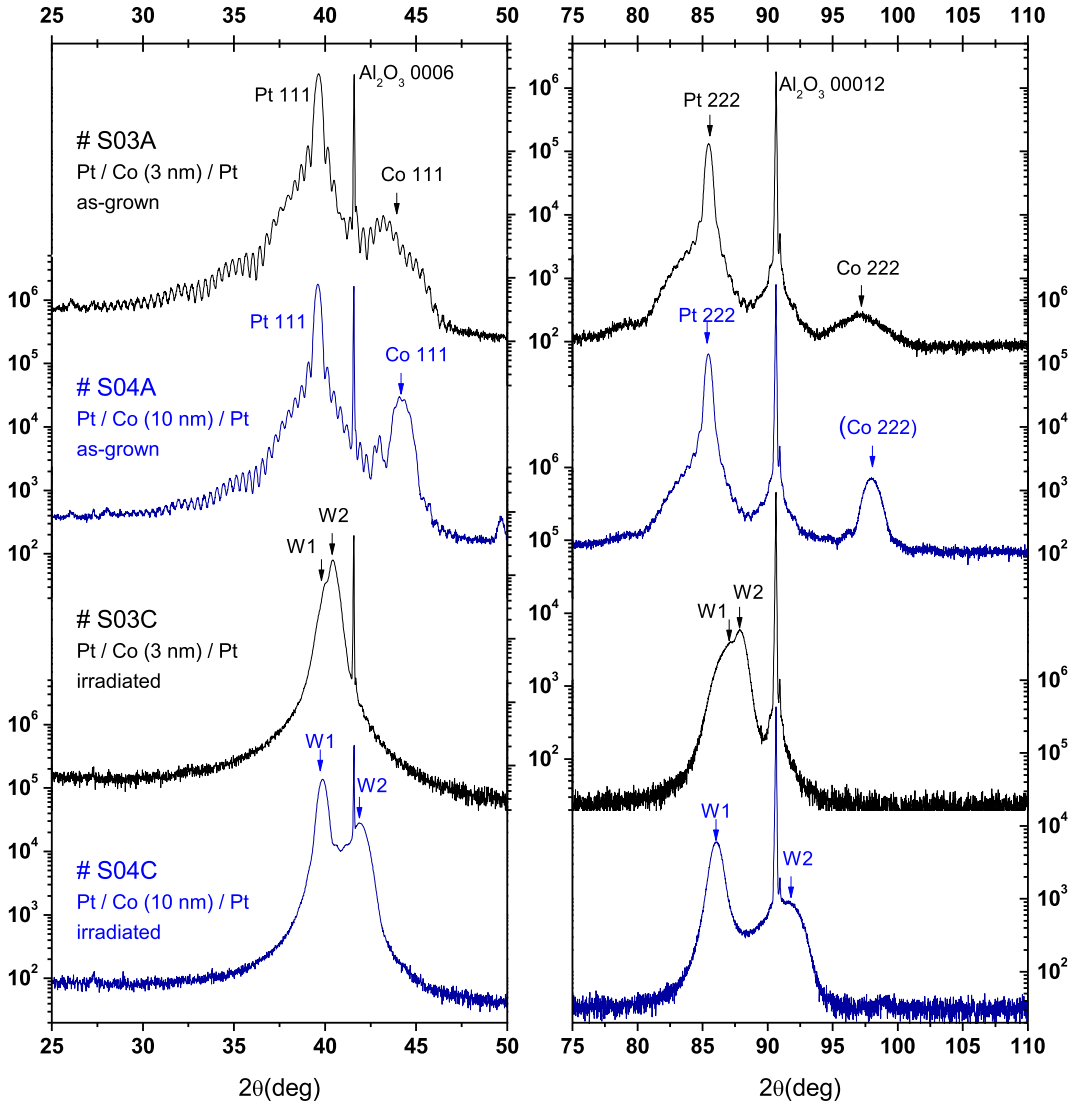

Fig. 2. Symmetric XRD patterns of S03 and S04 samples. See description in the text.

Table 2
Symmetrical and asymmetrical lattice spacing, lattice parameters of the relaxed cubic unit cells, compositions of the $Pt_{1-x}Co_x$ alloys and strain states of the layers obtained as a results of X-ray diffraction measurements of as grown and irradiated S03 - (25 nm Pt)/(3 Co)/(3 nm Pt) and S04 - (25 nm Pt)/(10 nm Co)/(3 nm Pt) samples.

Sample	Lattice spacing d_{222} (Å)	Lattice spacing d_{113} (Å)	Relaxed lattice parameter a_{rel} (Å)	Co atomic concentration in $Pt_{1-x}Co_x$ alloy x	Strain ε_{xx} ε_{zz} ($\pm 5 \times 10^{-4}$)
S03A	1.1345 (2)	1.1844 (2)	3.926 (4)	0	0 0
S03C	W_1: 1.1239 (2)	W_1: 1.1778 (2)	W_1: 3.930 (4)	W_1: 0	−0.0045 0.0090−0.0070 0.0140
	W_2: 1.1090 (2)	W_2: 1.1640 (2)	W_2: 3.895 (4)	W_2: 0.12 (2)	
S04A	1.1346 (2)	1.1849 (2)	3.930 (4)	0	0 0
S04C	W_1: 1.1280 (2)	W_1: 1.1800 (2)	W_1: 3.923 (4)	W_1: 0	−0.0025 0.0040
	W_2: 1.0736 (2)	W_2: 1.1262 (2)	W_2: 3.763 (4)	W_2: 0.54 (2)	−0.0060 0.0120

the top Pt layer and the whole samples surface. The initially sharp interfaces between the adjacent layers broaden due to material mixing after a single shot irradiation (middle row). Accumulation of more shots, here 10, makes the whole structure alloy over almost its total thickness (top row). The TEM results confirm the findings of XRD analysis concerning substantial mixing of the Co layer with adjacent Pt films. Irradiation with a single pulse causes already asymmetric mixing of the layers, with broader intermixing zone at the Pt-Co interface closer to the substrate (Fig. 3-N1). Close to the other interface we see a thin mixed Pt-Co sublayer with enhanced contents of cobalt. A multishot case (10 shots) is shown in Fig. 3-N10. In this case almost the whole amount of Pt and Co is roughly homogenized into a single Pt-Co alloy film.

The results of GIXR patterns fitting are shown in Fig. 4. For both *as grown* samples (S03A and S04A) a three-layer model was applied, while in case of irradiated samples, a bi-layer model was considered, based on the XRD results. The fitting procedure allows to determine the density and the thickness of deposited and

Table 3
Optimal parameters for GIXR model fits shown in Fig. 4 for sample series S03 and S04.

SAMPLE	Layer composition	Density g/cm^3	Thickness nm	Roughness nm	Concentration Co %
S03A	Pt	21.4	3.10	0.81	0
	Co	9.32	2.96	0.55	100
	Pt	21.4	24.64	0.16	0
	Al_2O_3	3.989	∞	0.16	
S03C	$Pt_{1-x}Co_x$ (W2)	19.66	26.47	0.79	16
	$Pt_{1-x}Co_x$ (W1)	21.04	5.01	5.06	4
	Al_2O_3	3.989	∞	0.17	
S04A	Pt	21.4	3.12	1.11	0
	Co	8.79	9.79	0.87	100
	Pt	21.4	26.04	0.21	0
	Al_2O_3	3.989	∞	0.18	
S04C	$Pt_{1-x}Co_x$ (W2)	14.4	17.82	0.55	60
	$Pt_{1-x}Co_x$ (W1)	21.4	21.80	2.43	0
	Al_2O_3	3.989	∞	0.14	

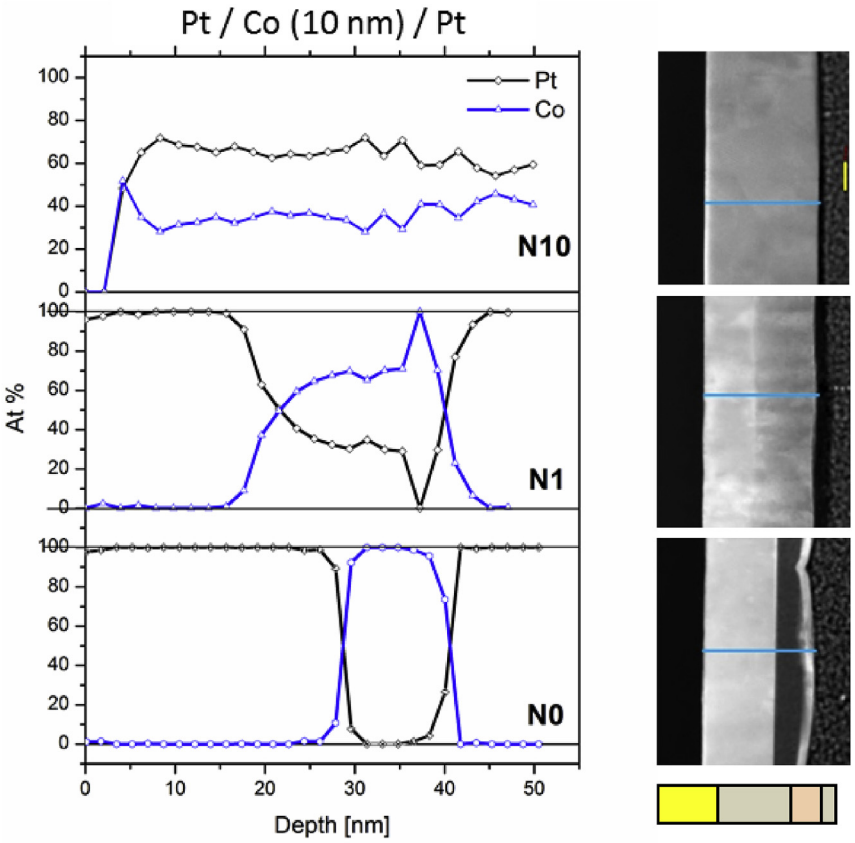

Fig. 3. EDX depth profiles (left) and TEM images of S04 sample parts (right): *as grown* (N0), and irradiated with 1 and 10 pulses of peak fluence 73 mJ/cm^2 (N1 and N10, respectively). Blue lines in the central part of images show approximate paths of EDX scan. Small vertical bar close to the right edge of a top picture scales to 10 nm distance. The sample structure profile is schematically shown at the bottom-right corner. (For interpretation of the references to colour in this figure legend, the reader is referred to the Web version of this article.)

irradiated layers as well as the interface roughness. The parameters which were optimized to fit GIXR models to experimental data are reported in Table 3. The obtained results are a in good agreement with other investigations, and particularly with the XRD measurements. The models resulting from GIXR fits were also applied to simulate the GIXRF data. The missing model parameters – average Co concentrations in layers – were calculated based on the density parameter [24]. The simulated GIXRF patterns for Co and Pt atoms are in a good agreement with the experimental data, apart from the S03C sample. In this case, the Co concentration in the top layer (deduced from the position of the W2 peak in XRD measurements) is too small to explain the GIXRF measurements. It may

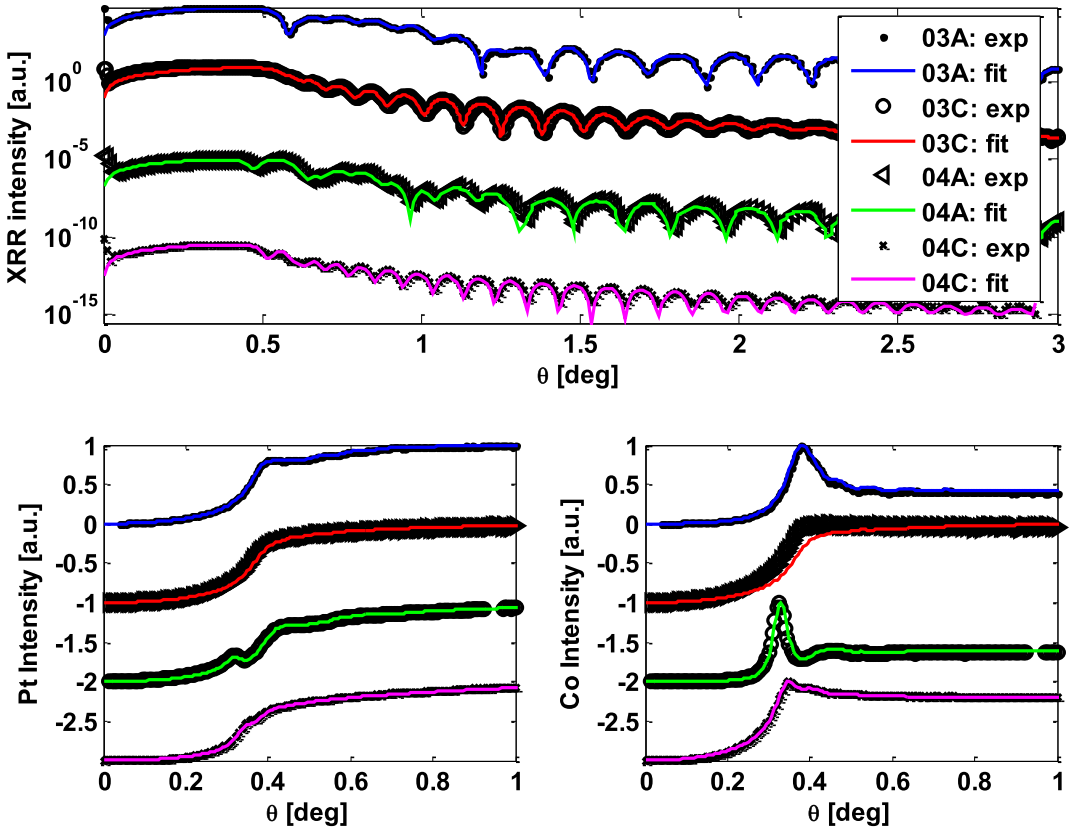

Fig. 4. GIXR (top) and GIXRF (bottom) of structures S03 and S04 together with optimal simulations with parameters shown in Table 3.

be caused by the fact that XRD technique "sees" only the coherent part of the crystalline structure, while GIXRF is sensitive to the elemental local field density and not to its lattice structure. A strongly disturbed (defected) thin surface layer reach on Co might not be detectable by XRD while it would have a significant impact on GIXRF patters. Secondly the sample volume probed by GIXRF is different from the one probed by XRD and GIXR methods due to smaller beam size at ELETTRA XRF beamline, fact which should be taken into consideration in case of quasi-uniform irradiated samples.

The EXAFS technique, similarly to GIXRF, is sensitive to the Co atoms independently of the layers crystalline structure. The EXAFS spectra in the normal and grazing incidences are very similar for respective samples (Fig. 5). Anisotropy does not manifest itself in a

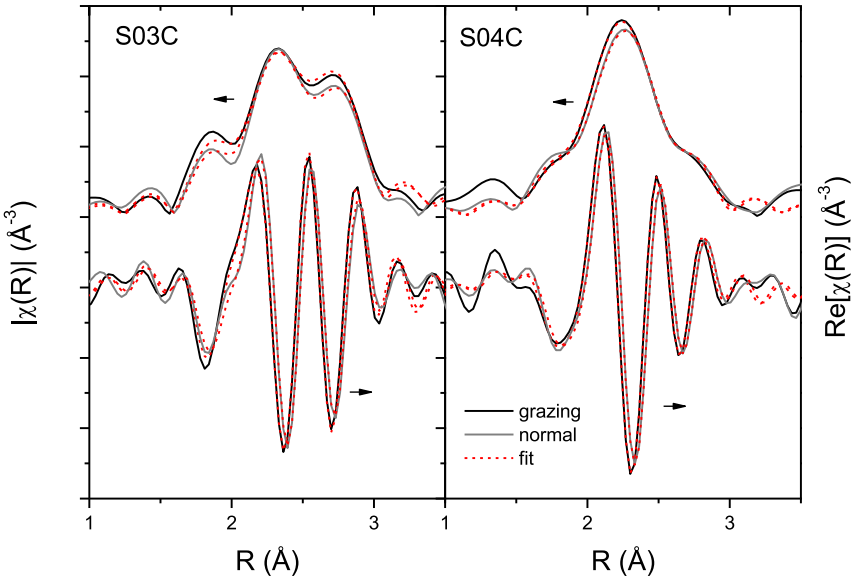

Fig. 5. The magnitude and real part of Fourier Transformed EXAFS oscillations for the S03C and S04C samples with their best fits. Spectra are shifted vertically for clarity.

distinct difference of EXAFS data shape but rather can be seen in the shift between the spectra which can be easier noticed looking on the real part of the FT EXAFS oscillations.

The analysis of the EXAFS spectra of the irradiated samples was performed using Demeter software [31] with POLARIZATION card. The spectra in both configurations (grazing and normal) were fitted simultaneously. The applied model is described in details in Ref. [29]. Following the XRD and XRR data, it takes into account that chemically disordered fcc Pt-Co alloy is formed after irradiation. The model assumes that the total number of neighbors in the first coordination shell stays equal to 12, while an additional parameter (x_{Co}) is introduced to describe the concentration of the Co atoms by the relationship: $N_{Co}{}^{*}x_{Co} + N_{Pt}{}^{*}(1\text{-}x_{Co}) = 12$, where N_{Co} - number of Co neighbors, N_{Pt} - number of Pt neighbors. Results of the EXAFS analysis are presented in Table 4. The found Co atomic concentrations are in agreement with the values obtained in XRD and XRR measurements for the top alloy layer in the irradiated samples (W2). In S03C sample, the Co concentration determined by EXAFS - 0.26 (8) is higher than from XRD – 0.12 but it is close to the best fit values of GIXRF – 0.30. As proposed above this may be related to the defects in the thin surface layer rich on Co. The EXAFS analysis shows that local atomic disorder parameter is relatively high for the Co atoms. It may be associated with the presence of defects like vacancies, since thermal disorder should be minimalized by sample's cooling during data acquisition. The Co-Co bond lengths in the alloys are higher than the ones obtained for the monoatomic (pure) crystalline structure (2.51 Å). Their values are correlated with the alloys composition (x_{Co}): the Co-Co bonds are getting longer while the Co atoms concentration decreases. In all cases the Co-Co and Co-Pt bond lengths in-plane are longer than these out-of-plane.

Table 4
Results of EXAFS fitting. R - bond length, σ^2 - local atomic disorder, x - concentration of the Co atoms in the first shell. "n" - normal configuration, "g" - grazing configuration.

	S03C	S04C
x Co	0.26 (8)	0.59 (7)
Co-Co		
σ^2_n [Å^2]	0.008 (5)	0.007 (1)
σ^2_g [Å^2]	0.010 (3)	0.007 (1)
R_n [Å]	2.69 (3)	2.62 (1)
R_g [Å]	2.64 (2)	2.60 (1)
Co-Pt		
σ^2_n [Å^2]	0.002 (1)	0.003 (2)
σ^2_g [Å^2]	0.002 (1)	0.003 (1)
R_n [Å]	2.71 (1)	2.65 (1)
R_g [Å]	2.69 (1)	2.63 (1)

The examples of P-MOKE maximal Kerr rotation images of S04 samples after spot and QU irradiations are shown in Fig. 6a and b, respectively. P-MOKE magnetization loops for *as grown* and QU irradiated samples are shown in Fig. 7. For S03 sample with initial cobalt thickness $d_{Co} = 3$ nm, the irradiation is strong enough to prompt out-of-plane magnetization, while for S04 sample with $d_{Co} = 10$ nm the irradiation induced increase of magnetic anisotropy was insufficient to cause out-of-plane magnetization. For spots irradiated with 1 and 10 pulses at the S04 sample, radial dependences of magnetic parameters (coercivity H_c, remanence θ_{REM}, and maximal Kerr rotation θ_{MAX}), shown in Fig. 8, indicate that magnetic modifications occur at distance below 0.4 mm from the spot center, which corresponds to the threshold energy density ~40 mJ/cm^2.

4. Conclusion

Structural modifications of the irradiated samples were studied by means of complementary techniques: XRD, GIXR, GIXRF, EXAFS and TEM. Our study revealed complexities in structure and magnetic order in the XUV-irradiated ultrathin Pt/Co/Pt films. We found that the platinum, in the two layers of *as grown* samples S03A and S04A, is relaxed, and the lattice parameter was calculated to be, a_{rel} (S03A) = 3.926 (4) Å and a_{rel} (S04A) = 3.930 (4) Å, slightly higher than the lattice parameter in a bulk Pt (a_{Pt} = 3.923 Å). In both quasi-uniform irradiated samples, on the other hand, we found approximately 1% tensile strain occurring in the $Pt_{1-x}Co_x$ alloy film. While in the *as grown* samples neither mixing of Co and Pt nor alloying of Pt-Co is observed, in both the irradiated samples the XRD patterns show near to the positions of the Pt 111 and Pt 222 peaks, two diffraction peaks very close to one another. The observed position of the peaks indicates an existence of two pronounced fractions of platinum rich $Pt_{1-x}Co_x$ alloys of different compositions. Experimental GIXR and GIXRF curves can be simulated precisely assuming segregated layers of Pt-Co-Pt with suitably modeled interfaces. The analysis of the EXAFS data indicates that at a presence of Co rich alloy layer under strain in the irradiated samples, as well. Thus, XRD, EXAFS, GIXR and GIXRF results support the conclusion that two distinct layers form two different pronounced films $Pt_{1-x}Co_x$ alloys with different Co concentration. At the same irradiation conditions, the final film composition of the sample is dependent on the thickness of *as grown* magnetic Co film. The TEM results

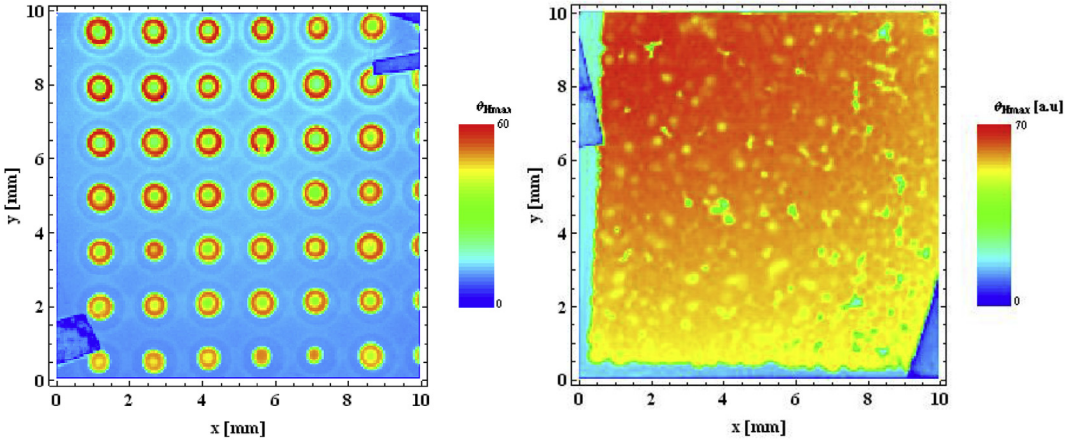

Fig. 6. PMOKE maximal Kerr rotation images of the samples after irradiation: (left) sample S04B after spot irradiation with shot repetition number (in rows) N = 1, 2, 3, 5, 10, 50, 100 (from bottom to top); (right) sample S04C after single shot (N = 1) quasi-uniform "raster" irradiation with step 0.2 mm.

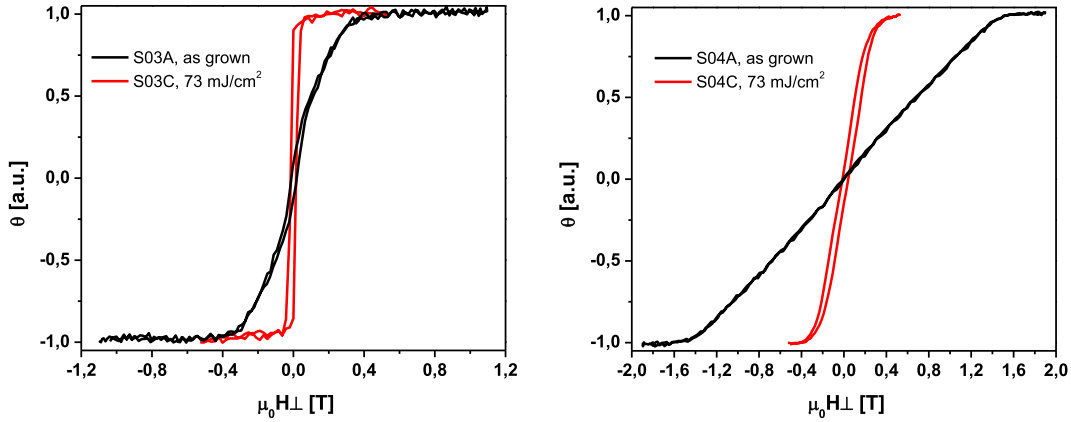

Fig. 7. PMOKE hysteresis loops measured for *as grown* and quasi-uniform irradiated samples S03 (left) and S04 (right).

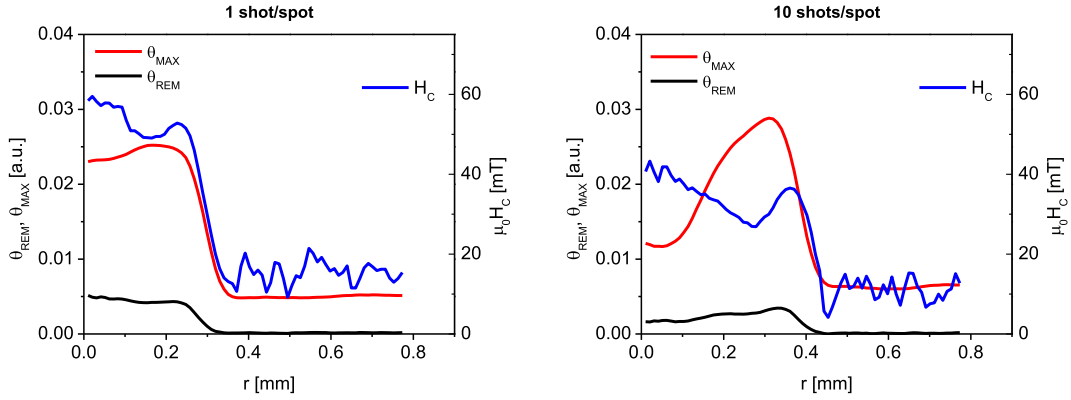

Fig. 8. Radial dependences of the maximal Kerr rotation θ_{MAX}, remanence θ_{REM} and coercivity H_C measured in the PMOKE configuration for the spots irradiated 1shot/spot (left) and 10 shots/spot (right) of the sample S04.

show that for smaller irradiation dose (lower number of pulses), only partial interdiffusion at the interfaces takes place. As a result, a tri-layer is formed with Pt-Co alloy in between Pt layers. In all studied cases the atomic mobility in the solid state, even above the activation temperature of approximately 450 °C [32], is not fast enough for the materials intermixing over a range of several nanometers in a short time (in the order of 1 μs) before the sample cools down to room temperature. Following the arguments presented in Ref. [33] one can conclude that the alloys formation due to atomic diffusion occurs when one of the materials melts (Co has lower melting temperature than Pt), which abruptly increases the atomic mobility over many orders of magnitude.

The difference in magnetic properties of the irradiated samples with different initial Co layer thickness (S03C and S04C) can be connected to their difference in the final $Pt_{1-x}Co_x$ alloy composition, because other parameters (lateral strain and alloy thickness) do not differ too much. Taking into account the dependence of saturation magnetization in $Pt_{1-x}Co_x$ alloy on Co concentration [34] one can conclude that out-of-plane magnetization for S03C sample can be obtained thanks to significant reduction of demagnetization factor for low Co concentration.

Acknowledgments

This work has been supported by the Polish National Science Center (Grant No. DEC-2012/06/M/ST3/00475) and by the EU FP7 EAgLE project under the grant agreement REGPOT-CT-2013-316014, co-financed by the Polish Ministry of Science and Higher Education, Grant Agreement 2819/7.PR/2013/2. Part of X-ray results has been obtained in the frame of the Project No. 20150487 at ELETTRA MCX station (XRD) and Project No. 20150518 at ELETTRA XRF station. We acknowledge the Elettra facility and staff for providing the access to the MCX beamline and the X-ray Fluorescence beamline. The research leading to these results has received funding from the European Community's Seventh Framework Programme (FP712007-2013) under grant agreement No. 312284 (CALIPSO). We acknowledge the European Synchrotron Radiation Facility for the provision of synchrotron radiation facilities and we would like to thank Dr. Angela Trapananti for assistance in using beamline BM08.

References

[1] Y.P. Lee, R. Gontarz, Y.V. Kudryavtsev, Phys. Rev. B 63 (2001), 144402.
[2] O. Rader, E. Vescovo, J. Redinger, S. Blügel, C. Carbone, W. Eberhardt, W. Gudat, Phys. Rev. Lett. 72 (1994) 2247.
[3] W.J. Antel Jr., M.M. Schwickert, T. Lin, W.L. O'Brien, G.R. Harp, Phys. Rev. B 60 (1999) 12933.
[4] C.L. Canedy, X.W. Li, G. Xiao, Phys. Rev. B 62 (2000) 508.
[5] B.N. Engel, C.D. England, R.A. Van Leeuwen, M.H. Wiedmann, C.M. Falco, Phys. Rev. Lett. 67 (1991) 1910.
[6] O. Robach, et al., Phys. Rev. B 65 (2002), 054423.
[7] J.-W. Lee, J. Kim, S.-K. Kim, J.-R. Jeong, S.-C. Shin, Phys. Rev. B 65 (2002), 144437.
[8] J.C.A. Huang, L.C. Wu, A.C. Hsu, Y.M. Hu, T.H. Wu, C.H. Lee, Phys. Rev. B 59 (1999) 1209.
[9] S.-B. Choe, S.-C. Shin, Phys. Rev. Lett. 86 (2001) 532.
[10] H. Brandle, D. Weller, J.C. Scott, S.S.P. Parkin, C.-J. Lin, IEEE Trans. Magn. 28 (1992) 2967.
[11] B. Heinrich, J.A.C. Bland, Ultrathin Magnetic Structures, Springer, Berlin, 1994.

[12] R.T. Heap, S.J. Greaves, J. Phys. D. 27 (1994) 1343.
[13] A. Maziewski, et al., Phys. Status Solidi A 211 (2014) 1005.
[14] C.-H. Lambert, et al., Science 345 (2014) 1337.
[15] R. Medapalli, et al., Phys. Rev. B 96 (2017), 224421.
[16] J. Kisielewski, et al., J. Appl. Phys. 115 (2014), 053906.
[17] A. Maziewski, et al., Phys. Rev. B 85 (2012), 054427.
[18] C. Chappert, et al., Science 280 (1998) 1919.
[19] T. Devolder, Phys. Rev. B 62 (2000) 5794.
[20] T. Devolder, S. Pizzini, J. Vogel, H. Bernas, C. Chappert, V. Mathet, M. Borowski, Eur. Phys. J. B 22 (2001) 193–201.
[21] J. Jaworowicz, et al., Appl. Phys. Lett. 95 (2009), 022502.
[22] M. Sakamaki, et al., Phys. Rev. B 86 (2012), 024418.
[23] C. Schuppler, et al., Appl. Phys. Lett. 88 (2006), 012506.
[24] E. Dynowska, et al., Nucl. Instrum. Meth. Phys. Res. B 364 (2015) 33–39.
[25] I. Sveklo, et al., J. Phys. D Appl. Phys. 50 (2017), 025001.
[26] A. Bartnik, et al., Nucl. Instrum. Methods Phys. Res. A 647 (2011) 125–131.
[27] A. Bartnik, et al., Appl. Phys. B 96 (2009) 727–730.
[28] B.L. Henke, E.M. Gullikson, J.C. Davis, Atomic Data Nucl. Data Tables 54 (1993) 181–342.
[29] A. Wolska, et al., Nucl. Instr. Meth. Phys. Res. B 411 (2017) 112.
[30] A.I. Benediktovich, I.D. Feranchuk, A. Ulyanenkov, Phys. Rev. B 80 (2009) 235315.
[31] B. Ravel, M. Newville, J. Synchrotron Rad. 12 (2005) 537.
[32] O. Ersen, C. Goyhenex, V. Pierron-Bohnes, Phys. Rev. B 78 (2008), 035429.
[33] A.R. Khorsand, et al., Optic Express 18 (2010) 700.
[34] D. Weller, H. Braendle, C. Chappert, JMMM 121 (1993) 461.